

# Thermal Investigations on a CNC Lathe Fitted with a Dynamically Enhanced Steel-Reinforced Epoxy Granite Bed

Mula Venkata Ramana<sup>1,\*</sup> – Pudukarai Ramaswamy Thyla<sup>1</sup> – Subramanian Elango<sup>2</sup> – Chinnuraj Shanmugam<sup>1</sup>

<sup>1</sup>PSG College of Technology, Department of Mechanical Engineering, India

<sup>2</sup>Galaxy Machinery Pvt Ltd, India

*Polymer concrete or epoxy granite is becoming more popular for beds, bases, and other structures of precision machine tools, owing to its excellent damping characteristics. To realize the same static rigidity as that of the cast-iron structures, steel-reinforced epoxy granite (SREG) structures are being used. The vast differences in the thermal properties of steel and epoxy granite (EG) are likely to cause higher magnitudes of thermal error. This work aims to investigate the thermal behaviour of a computerized numerical control (CNC) lathe built with a novel dynamically enhanced SREG bed and compare its performance with the lathe with a cast iron bed. Experimental and numerical investigations have been carried out under cross-feed (CF) drive idle running conditions to determine the TCP deformation. The results reveal that the thermal error in the CNC lathe with SREG bed is 1.68 times that of the lathe with cast iron (CI) bed at 20 °C and 1.8 times at 40 °C environmental temperature variation chamber (ETVC) conditions. It could be identified that the heat generated in the CF is conducted to the steel guideways embedded in the SREG bed, but further heat transfer to the EG portion of the bed is impeded, and hence the heat accumulation that occurs in the guideways leads to higher magnitude of the thermal error. The experimentally validated numerical model is used to extend the investigations to study the effect of the idle running of the longitudinal feed drive (LF) and combined cross and longitudinal feed drives, on the thermal behaviour of the lathe.*

**Keywords:** precision machine tools, thermal error, steel reinforcement, epoxy granite

## Highlights

- The use of steel reinforcements in epoxy granite for machine tools is an innovative attempt to achieve the same stiffness as CI machine tool structures with enhanced damping characteristics.
- This research work aims to investigate the thermal error in a CNC lathe with an SREG bed and compare it with the thermal error in a CNC lathe with a CI bed.
- Thermal error in the CNC lathe with SREG bed is 1.68 times that of the lathe with CI bed at 20 °C and 1.8 times at 40 °C environmental temperature variation chamber (ETVC) conditions.
- A finite element model (FEM) has been developed, and the simulation results are well in agreement with the experimental results.

## 0 INTRODUCTION

Machining accuracy is a crucial parameter in the development of precision machines. Since machine tool performance is governed by static, dynamic, and thermal stability, designers must contemplate these aspects at every stage of development [1] and [2]. Different materials with desired properties are used for various machine tool components. Cast iron (CI) is commonly used as a material for the base or bed since they are essential parts that hold all the other parts together and also can absorb shocks and vibrations [3] and [4]. Instead of CI, mineral castings such as tailor-made polymer concrete (PC) materials have gained popularity in recent years for use in high-performance and high-speed machine tools to ultra-precision machines and metrology applications due to their excellent damping characteristics [5] to [7].

Mineral castings are light in weight and require lower development and handling costs. A wide range of polymers and particulates have been used

to develop custom-made polymer concrete for machine tool structures [8] and [9]. Epoxy granite (EG) is a type of tailor-made material that belongs to the polymer concrete group [10]. A suitable epoxy granite mix proportion can be chosen by optimizing several parameters, such as the type and content of the resin and filler, curing method, curing temperature, humidity, and, most importantly, the resin-to-filler ratio and matrix-to-aggregate ratio, which influence the characteristics of epoxy granite [11].

EG has a significantly high damping capacity due to the high viscoelasticity of the epoxy resin and a damping ratio that is seven to ten times that of conventional cast iron; however, it has a low modulus of elasticity [12]. EG is used as a machine tool structural material to improve dynamic performance by increasing stiffness with fibre addition, applying form design principles to structures, and embracing metal reinforcements [13] to [15]

Suh and Lee [16] developed a hybrid steel and polymer concrete bed, which was also incorporated

\*Corr. Author's Address: 1PSG College of Technology, Department of Mechanical Engineering, India, venkataramana048@gmail.com

into a high-speed gantry-type milling machine. The dynamic performance revealed that the hybrid polymer concrete exhibited superior damping characteristics, with damping ratios ranging from (2.93 % to 5.69 %) when compared to existing cast-iron beds with damping ratios ranging from (0.2 % to 0.3 %).

EG structures are capable of replacing existing CI structures for bed and base applications; In such cases, it is critical to maintain the footprints of the traditional CI bed to meet assembly requirements. Metal reinforcements are an alternative to making significant form design changes to enhance static stiffness whilst also meeting footprint requirements [17]. Chinnuraj et al. [17] presented the static and dynamic characteristics of a computerized numerical control (CNC) lathe with a CI bed and SREG bed. Experiments revealed that the dynamic performance of the lathe with an SREG bed improved considerably compared to that of the lathe with a CI bed.

Another advantage of EG is that its thermal conductivity is very low, which aids in maintaining thermal stability under different climatic conditions associated with environmental temperature variations [18] and [19]. However, it is vital to investigate the total machine tool's thermal behaviour and the thermal error under the influence of heat generated internally due to friction in bearings, guideways, and other moving assemblies. Thermal error accounts for 30 % to 70 % of the overall error in machine tools [20] and [21]. Although EG is thermally stable, since it is reinforced with steel whose thermal conductivity is much higher than that of EG, a bi-material effect can arise as the temperature of the machine tool rises and heat flows through the reinforcement in EG structures, resulting in thermal error.

Suh and Lee [22] investigated the thermal characteristics of steel and polymer composite sandwich structures for high-speed milling machines using finite element model (FEM) analysis and experiments to ensure that vertical column deformation was permissible given the allowable deformation for proper linear motor operation.

The objective of this work is to study the influence of the bi-material effect (different thermal properties) of steel and EG on the thermal behaviour of the lathe, in comparison to that of the lathe with the existing cast iron bed. In this work, investigations on the thermal behaviour of a CNC lathe built with an SREG bed have been carried out as a continuation of the static and dynamic investigations of this lathe presented by Chinnuraj et al. [17]. The thermal error associated with SREG structures must be investigated in order to obtain the full benefits of the thermally

inert, high damping tailor-made EG material. Some feasible methods of reducing thermal error have prompted the use of EG material in precision machine tools. According to Tanabe and Takada [23], heat sources should be kept separated from polymer concrete structures in machine tools in order to reduce large thermal gradients.

Neugebauer et al. [24] reduced thermal error in a machine tool built with a mineral casting bed by isolating heat sources by providing a composite layer of different materials with different thermal expansion coefficients. Weidlich and Nestmann [25] studied thermal deformations in a polymer concrete bed caused by local temperature gradients and provided additional steel fixings in linear guideways to improve heat conduction; investigations into such a method revealed a 30 % reduction in deformation.

This paper presents the thermal behaviour of a CNC lathe fitted with a novel dynamically enhanced SREG bed in place of the conventional cast iron bed. Numerical models of the lathe with the original CI bed as well as the lathe with the newly proposed SREG bed have been developed and validated with experiments. The thermal conductivity of epoxy granite is nearly 1/30<sup>th</sup> of that of steel. When steel reinforcement is embedded inside epoxy granite, the vast differences in their thermal properties will contribute to high thermal contact resistance at the interface. To improve the accuracy of the numerical model, joint contact resistance has been incorporated between the steel reinforcement and epoxy granite by adopting the joint contact resistance proposed by Brahma et al. [26]. To highlight the benefits of SREG structures for machine tools, brief insights on the static and dynamic analysis of lathe bed, Vertical Machining Centre (VMC) base, and VMC column have been explained in Section 2. Experimental investigations on the thermal behaviour of CNC lathe with CI and SREG beds have been presented in Section 3. The development and validation of the numerical model have been discussed in Section 4. The validated numerical model has been used to determine thermal error under the idle running of longitudinal feed drive and idle running of both cross and longitudinal feed drives, and conclusions have been made and presented in Sections 5 and 6, respectively.

## 1 LITERATURE REVIEW

Cutting forces induce twisting and bending of the machine tool structures; therefore, the machine tool bed/base/column must be rigid against both bending loads and twisting moments. This section

contains an overview of the literature on the use of steel reinforcement to obtain equal stiffness for EG machine tool structures.

Dunaj et al. [27] and [28] developed lightweight steel-polymer concrete frames that have a 239 % improvement in modal damping ratio and 83 % less weight than a steel frame for a vertical lathe to improve machining stability. The performance of a lathe with a steel-polymer concrete frame revealed that the static stiffness of the lathe steel support system is increased by 30 % and an 83 % (on average 55 %) reduction in relative tool-workpiece frequency response function amplitudes when compared to the steel variant.

Chinnuraj et al. [17], Venugopal et al. [29] and [30] carried out investigations on the application of SREG structures to CNC lathe and VMC. Static and dynamic investigations have revealed that the use of SREG structures in machine tools will enhance the static and dynamic performance of the machine. The authors developed numerical models of the structures and validated the same through experimental modal analysis; these validated models aid in the iterative design of steel reinforcements and the EG structure. Based on the numerical investigations, the best reinforcement design was chosen from among several proposed designs. SREG structures for CNC lathe and VMC with the best design configuration were fabricated and tested for static stability and modal frequencies. The results revealed that the SREG structures have higher stiffness and natural frequencies than the respective CI machine tool structures, with significantly lesser mass. The material properties of steel, cast iron, and EG are represented in Table 1.

**Table 1.** Machine tool structures material properties

Property	Material		
	Steel	Cast iron	Epoxy granite [15]
Density, [kg/m <sup>3</sup> ]	7800	7250	2300
Modulus of elasticity, [GPa]	210	110	30
Poisson's ratio	0.27	0.24	0.25
Compressive strength, [MPa]	250	600	110
Flexural strength, [MPa]	380	450	36
Damping ratio	0.0001	0.001	0.0176
Thermal conductivity, [W/(m·K)]	45 to 50	50	0.5 to 1.5
Thermal expansion coefficient, [°C]	12x10 <sup>-6</sup>	6x10 <sup>-6</sup>	12x10 <sup>-6</sup>
Heat capacity, [J/(kgK)]	460	460	700

The results of the static and dynamic analysis carried out on the SREG structures of the CNC lathe and VMC, with the finalized reinforcement configuration are presented in Table 2. Chinnuraj et

al. [17] developed five design configurations for the steel reinforcement and developed the SREG bed with design configuration #5 among all designs, as shown in Fig. 1, which improved torsional stiffness, and provided a significant positive shift in natural frequencies and 22 % mass reduction as compared to CI bed. The torsional rigidity of the SREG bed was found to be 3.3 times that of the original CI bed. The developed SREG bed was fabricated, and the numerical model was validated by conducting static and modal testing.

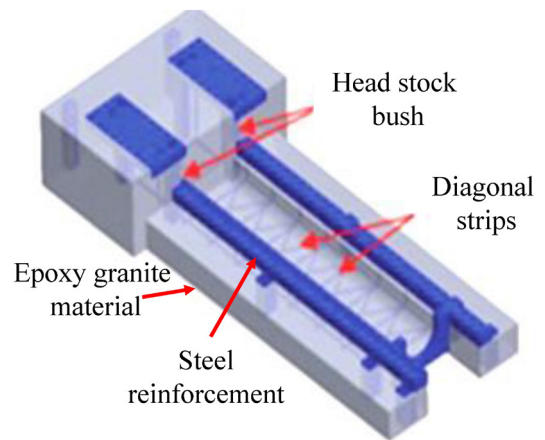


**Fig. 1.** Steel-reinforced epoxy granite (SREG) bed

Table 2 contains a review of the literature comparing the static dynamic characteristics of SREG or hybrid structures (steel and polymer concrete structures) to conventional structures.

Even though the static and dynamic characteristics of the SREG bed or hybrid structures have been proven to be superior to those of the original CI bed, the behaviour of the SREG bed to thermal loads needs to be investigated. There is a possibility of a bi-material thermal effect due to large changes in their operating conditions, ranging from extremely heavy loads encountered in rough machining cycles to extremely light loads encountered in finishing cycles. The results will aid in reconfiguring the reinforcement design to enhance heat transfer, thus reducing thermal error.

## 2 EXPERIMENTAL INVESTIGATIONS ON THE THERMAL BEHAVIOUR OF CNC LATHE WITH CI AND SREG BEDS

### 2.1 Experimental Procedure

As shown in Fig. 2, a CNC lathe was taken up for investigations on its thermal behaviour. The length

**Table 2.** Static rigidity and modal parameters of CI and SREG structures

Literature reference	Findings from static analysis			Findings from dynamic analysis				Mass of the developed structure [kg]		
	Parameter measured in developed structure	Parameter magnitude		First natural frequency [Hz]		Average damping ratio of structure		CI or Existing structure	SREG or hybrid structure	
		CI or Existing structure	SREG or hybrid PC	CI or Existing structure	SREG or hybrid PC	CI or Existing structure	SREG or hybrid PC		EG portion	Steel reinforcement
Chinnuraj et al. [17]	Torsional rigidity of the lathe with different beds [Nm/arc.s]	7.32	11.7	258	276	0.0007	0.004	110	67	19
Venugopal et al. [29]	Deformation along y-direction in VMC base [ $\mu\text{m}$ ]	18.8	12.1	133	370	0.0013	0.005	890	1041	64
Venugopal et al. [30]	Deformation at the spindle nose in VMC column [ $\mu\text{m}$ ]	76.8	75.2	92	89	0.001	0.004	660	542	161
Dunaj et al. [27] and [28]	Lightweight steel-concrete frame for vertical lathe	-	-	18.8	19.2	0.0008	0.002	1338	Variant 1: 1667 Variant 2: 1775 Variant 3: 1705	
Xu et al. [31]	Deformation of Steel-fiber Polymer Concrete (SFPC) lathe bed	0.21	0.41	143	165	0.003	0.04	-	-	-
Suh, J.D., Lee, D.G. [16]	Deformation of the machine tool bed under inertia and attraction forces [ $\mu\text{m}$ ]	-	48.8	-	93	0.002 to 0.003	0.029 to 0.056	-	-	-
Chen, T.C. [32]	Z-axial static stiffness [ $\text{N}/\mu\text{m}$ ]	330	286	98	240	0.0015	0.03	-	-	-

( $L$ ) and breadth or width ( $W$ ) of the bed fitted in the lathe are 975 mm and 344 mm. The distance from the bed bottom to the top surface ( $H$ ) is 405 mm. The dimensions of the machine tool are shown in Fig. 2. To provide the same information for measuring, pre-experiment adjustments, and corrections must be made precisely. The assumptions considered in this analysis are:

1. The effect of machining is not considered since a large amount of cutting liquid is required in the machining process; thermal deformation between the cutting tool and the parts being machined is ignored [33].
2. Since machining is not considered, the effect of chips is not factored.
3. The offset errors of the ball screws are already corrected by the controller parameters.
4. Since the experiments are carried out in a closed environment chamber, the environmental impact, such as magnetic field, humidity change, and vibration, is ignored since the primary objective of the research is to identify the discrepancy in CNC lathe performance with different beds.

Since TCP on the lathe turret is primarily associated with the moment of feed drives, the thermal behaviour of the feed drive has been considered separately to analyse its impact on the use of the SREG bed on TCP, which is prompted by the axis thermal growth of the feed drive. Methods for a systematic examination of the thermal behaviour of machine tools are provided by the International Organization for Standardization (ISO 230-3) [34].

The loading cycle considered for thermal analysis is three minutes running and one minute idle. The different machining operations carried out on the machine tool require fluctuating load cycles [33]. As per standards [34], the feed drive should run for 6 hours at the specified load cycle. The drive system's feed is to idle run at a maximum speed of 20 m/min for three minutes and stop for one minute. The load cycle is used to investigate the transient temperature variations in the machine structure as a result of intermittent and repeated machining circumstances.

Temperature sensors, RTD Pt100 as shown in Fig. 4c are used for temperature measurement by gluing them to different critical machine elements.

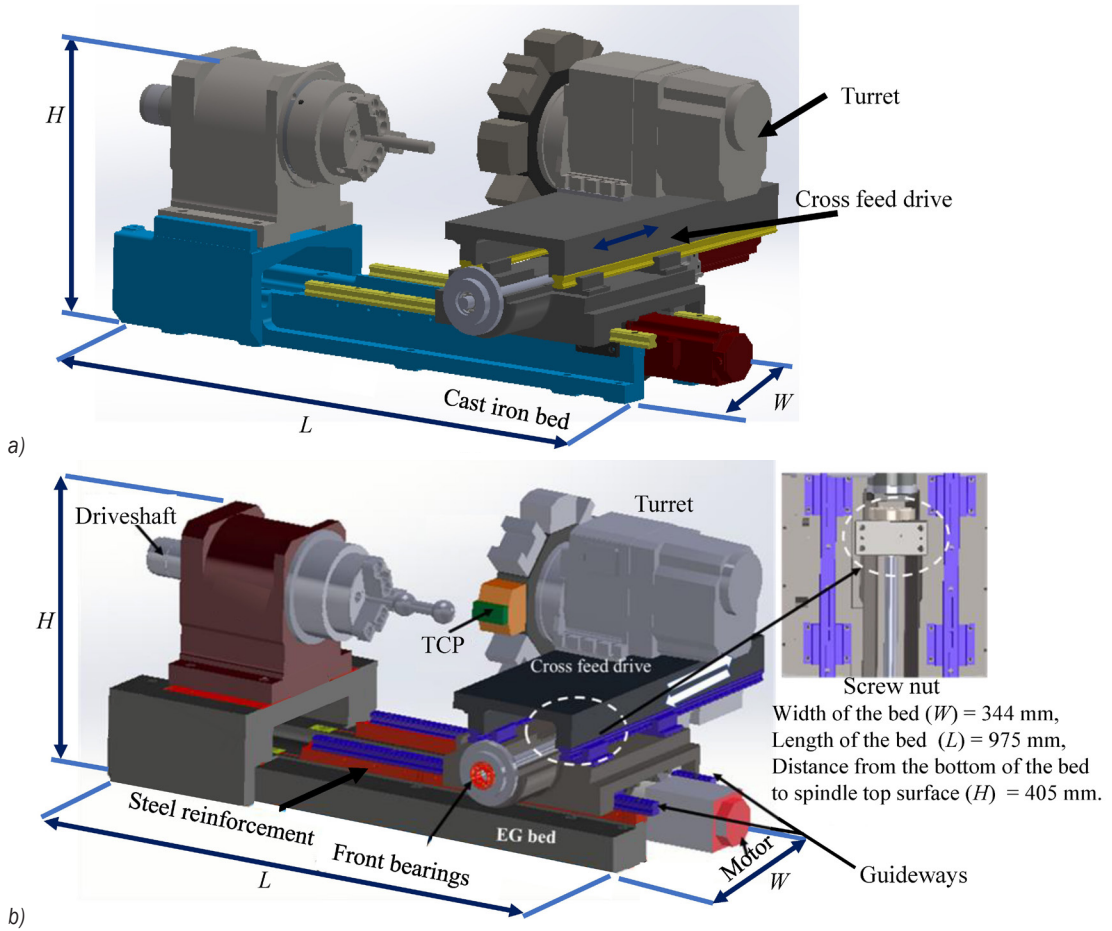


Fig. 2. a) CNC lathe with CI bed, and b) CNC lathe with SREG bed

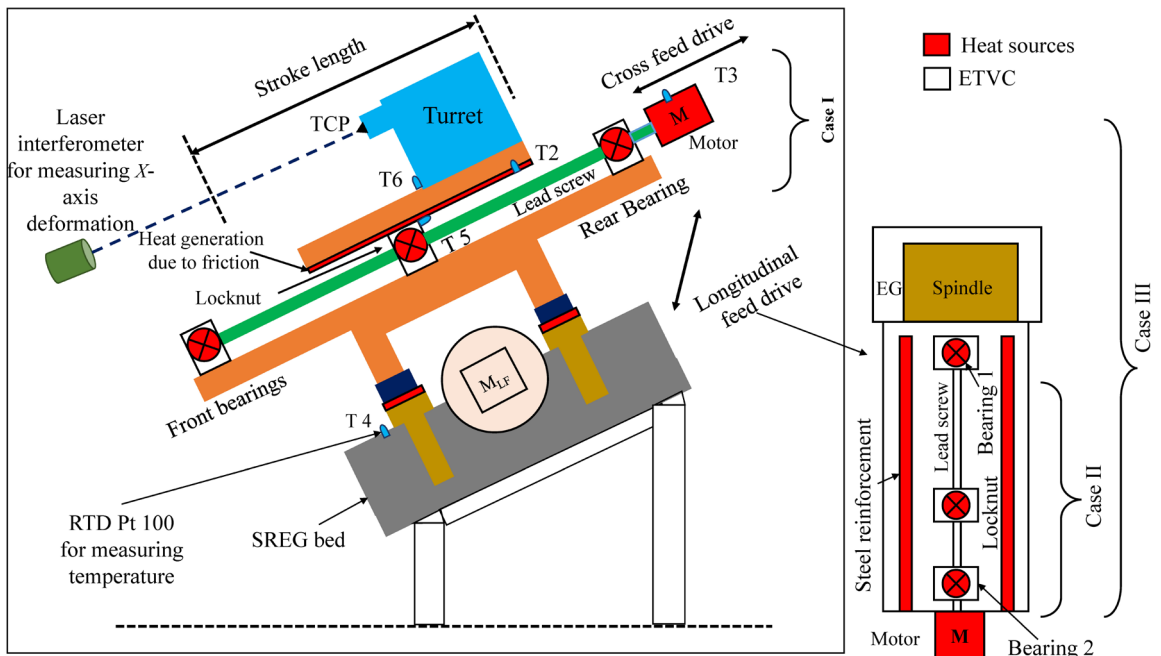


Fig. 3. Schematic representation of experimental setup

Since major heat sources are in motion during experimentation, a few sensors were mounted at critical locations, as shown in Table 3. A laser interferometer (Make: Renishaw XL80) is used to measure the x-axis thermal growth measurement. The XL-80 environmental compensation unit is attached to the sidewall surface of the machine tool casing as shown in Fig. 4 in order to minimize the influence of temperature and air pressure variation in laser interferometer measurement. The location of temperature and deformation sensors are represented in Fig. 3. Temperature data is collected every minute, and deformation is collected every 15 minutes by the data acquisition system (DAQ).

In order to make a meaningful comparative study of the effect of using the SREG bed against the CI bed in CNC lathe, the thermal deformation of structures arising due to ambient temperature variations has to be eliminated by conducting the experiments under identical controlled environments. Firstly, the experiments were carried out on the lathe, which was

originally built with a cast iron bed, with the cross-feed drive idle running. Secondly, the studies were repeated on the lathe with a newly developed SREG bed instead of a cast iron bed as shown in Fig. 4.

The machine tool has two feed drives: cross feed (CF) drive and longitudinal feed (LF) drive. Since the standard testing procedure for the lathe with the original CI bed involves conducting experiments with the cross-feed drive idle running, the lathe with the SREG bed is also run with the cross-feed drive idle running. Experimental investigations were carried out at 20 °C and 40 °C, to simulate typical operating conditions, below and above room temperature. Firstly, the lathe with a CI bed is moved to an ETVC chamber and maintained at a temperature of 20 °C. The machine is allowed to soak and experiments are conducted by running the cross-feed drive with a loading cycle. Temperature and x-axis deformation of TCP at one fixed end are measured during the experiment. After the experiment under 20 °C ETVC conditions, the lathe is soaked at 40 °C and

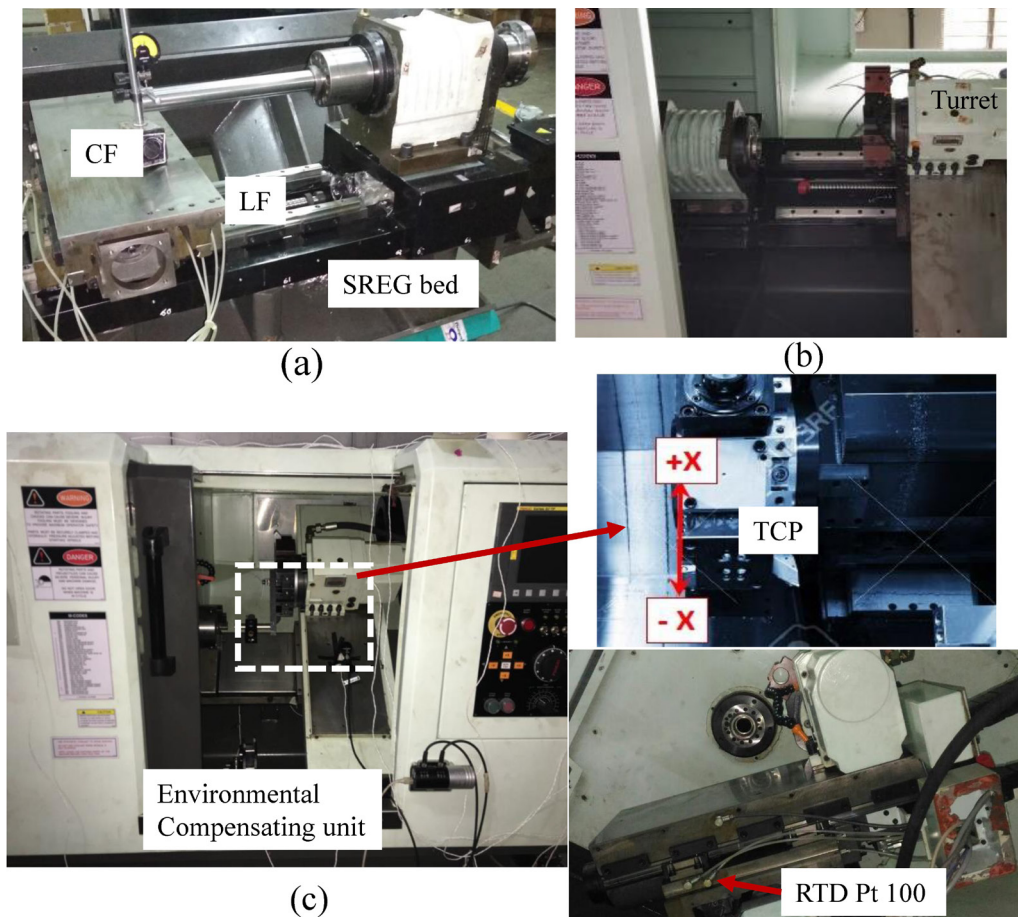


Fig. 4. a) Assembly of lathe with SREG bed, b) lathe with SREG bed, and c) experimental setup

the experiment was repeated. The CNC lathe is removed from the ETVC chamber, disassembled, and reassembled with an SREG bed. The experimental procedure is repeated on the CNC lathe with the SREG bed under both 20 °C and 40 °C ETVC conditions, similar to the lathe with the CI bed.

The soaking time required for the lathe with CI and SREG beds was found to be nearly the same, which is 4 hours for 20 °C and 7 hours for 40 °C environmental conditions. The heat from the heat sources is conducted to the surrounding structures, thus causing a thermal gradient in the machine tool structures. In such cases, the developed non-uniform temperatures could lead to expansion of structures resulting in thermal error. In Fig. 4, notations +X and -X refers to distances away from and towards the operator respectively.

### 2.2 Analysis of Thermal Behaviour under Cross-Feed Drive Idle Running

The temperature measured from experiments at various sensor locations glued on the lathe with the CI bed and the SREG bed at 20 °C and 40 °C is depicted in Figs. 5 and 6, respectively.

T1 represents the ambient temperature and the variation of the same is limited to 0.5 °C. Similarly, T2, T3, T4, T5, and T6 represent the temperatures at the LM block, drive motor, bed centre, ball screw housing, and turret. Since T2 and T3 represent the temperature in the vicinity of heat sources, they are found to be higher in magnitude in all the experiments.

Transient variation of X-axis thermal growth can be considered as a measure of thermal error. Transient variation of feed drive drifts in the lathe with a CI bed and SREG bed at 20 °C and 40 °C environment temperatures are analysed and the same is depicted

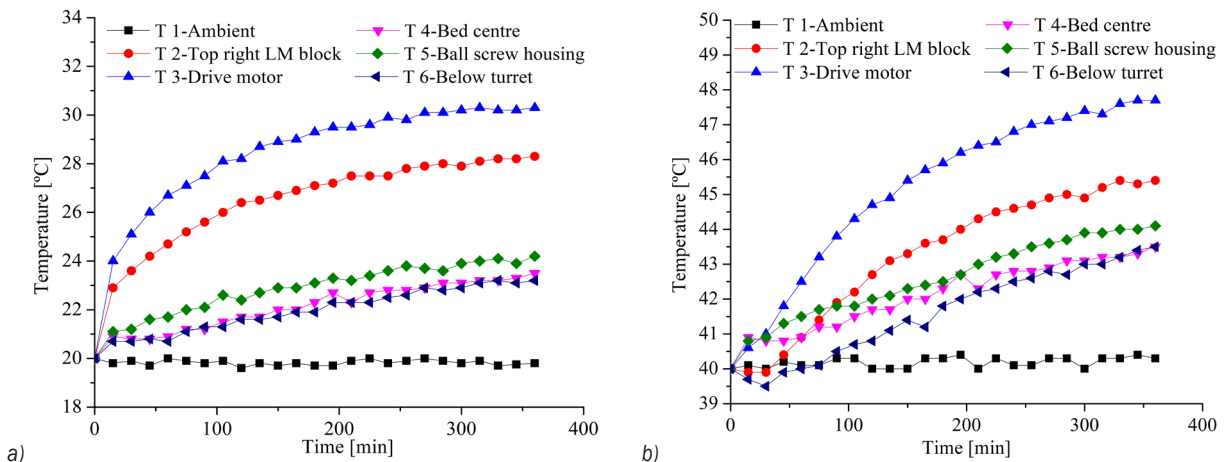


Fig. 5. Transient variation of temperature in the lathe with CI bed at a) 20 °C, and b) 40 °C environment temperature

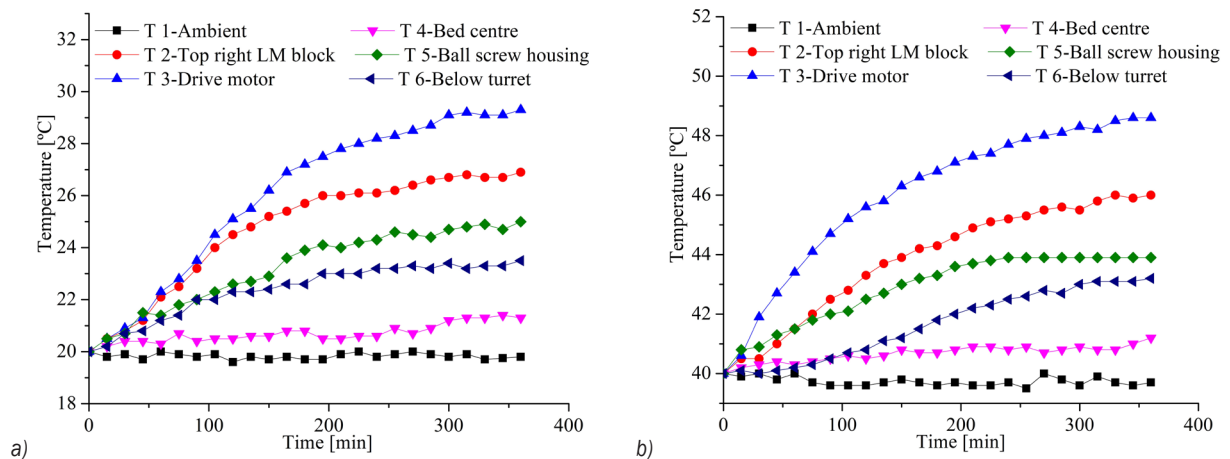


Fig. 6. Transient variation of temperature in the lathe with SREG bed at a) 20 °C, and b) 40 °C environment temperature

in Fig. 7. The trend of variation of the x-axis growth observed under 20 °C and 40 °C environment temperature conditions show the behaviour of the machine tool typically at temperatures below and above room temperature. Since the difference from 20 °C to room temperature and 40 °C to room temperature is not similar, a slight difference with a similar trend in the opposite direction has been observed in the lathe with both the CI bed and SREG bed.

From Fig. 6a, at 20 °C from 0 min to 360 min, the temperature difference of 8 °C, and 11 °C, have been observed at T2, and T3, respectively. From Fig. 6b, at 40 °C from 0 min to 360 min, the temperature difference of 7.5 °C, and 8 °C have been observed at T2, and T3, respectively. The change in temperatures of the structures is a higher magnitude of temperature difference observed at 20 °C than 40 °C, which refers to the rate of heat transfer being higher at 20 °C as compared to 40 °C. From the temperature profile, a maximum temperature difference has been observed in the drive motor and LM block locations in the first 120 min. From 120 min to 360 min, the rise in temperature is less which reflects a low-temperature difference. Therefore, the variation in x-axis thermal growth from 120 min to 360 min is low. The temperature of structures in the lathe with CI bed, from T2 to T6 reached steady-state reached after 120 min, whereas at 40 °C ETVc the steady-state has been identified after 300 min.

From Fig. 6b, the temperature profile of the lathe with CI bed at 40 °C, the temperature rises among T2 to T6 locations increased gradually. At 40 °C, the temperatures of the structures of the lathe with a CI bed are observed to be lesser than that in the lathe with an SREG bed. Therefore, the cumulative expansion

of all structures in the lathe with CI bed at 40 °C will be lesser than the cumulative expansion of the corresponding structures of the lathe with SREG bed at 40 °C. The results show that the temperature rise of the EG portion in the SREG bed is low owing to its very low thermal conductivity. A higher temperature rise has been observed in the lathe with SREG bed than that in the lathe with a CI bed, except in the bed itself. Figs. 7a and b compare the x-axis thermal growth in the CNC lathe with the CI bed at TCP to the x-axis thermal growth in the lathe with the SREG bed at 20 °C ETCV and 40 °C ETVc conditions, respectively. At 20 °C chamber conditions, the thermal growth at TCP is in the negative direction (towards the operator), and the trend followed was identical to that reported by Ruijun et al. [35], and Xu et al. [36]. At 40 °C chamber conditions, the thermal growth at TCP is in the positive direction (away from the operator), and the trend followed was identical to the observation in experiments conducted by Li et al. [37]. From Fig. 7, the x-axis growth in the lathe with the SREG bed is found to increase from 0 µm to 17 µm (towards the operator side) in the time span of 0 min to 150 min. Further, in the time span of 150 min to 225 min, the x-axis thermal growth is found to remain unaltered and then reversed from -18 µm to -14.8 µm in the time span of 225 min to 360 min. The start of the reverse trend is deemed as a sign of the development of re-initiation of unsteady-state due to non-uniform temperature.

From, Fig. 7a, at 20 °C ETVc conditions the linear x-axis thermal growth at 360 min in the lathe with CI bed is limited to -8.8 µm, whereas for the lathe with the SREG bed, it is -14.8 µm. Due to more heat accumulation in the steel reinforcement, which is

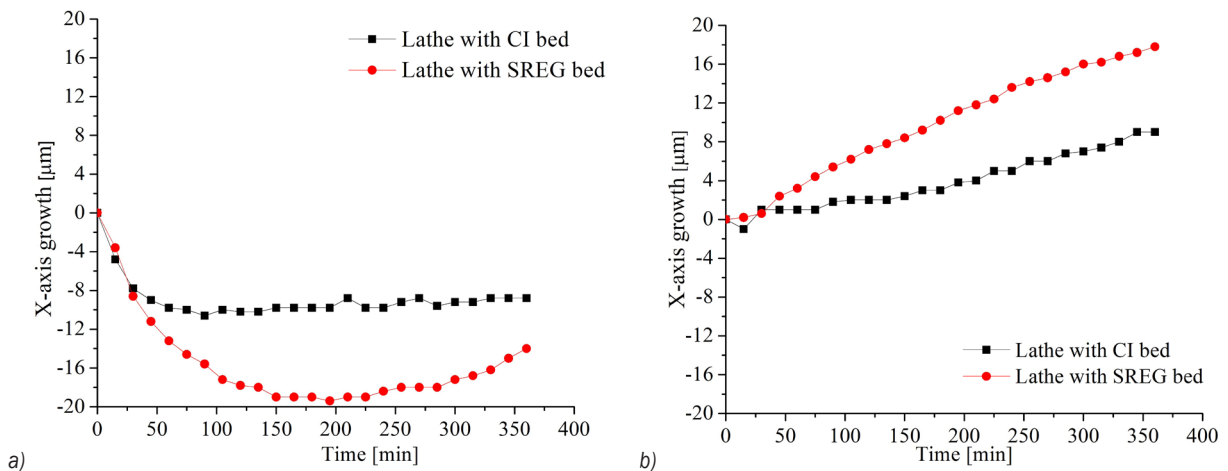


Fig. 7. Transient variation of x-axis feed drive drift at a) 20 °C ETVc, and b) 40 °C ETVc

reflected as the temperature rises in the lathe with the SREG bed, more nonuniform temperature distribution leads to more thermal error than in the lathe with CI bed at 20 °C.

From Fig. 7b, the  $x$ -axis thermal growth in the lathe with CI bed from 0 min to 340 min gradually increased from 0  $\mu\text{m}$  to 9  $\mu\text{m}$ . Further, from 340 min to 360 min not much variation exists in the  $x$ -axis thermal growth. The  $x$ -axis thermal growth in the lathe with SREG bed from 0 min to 360 min gradually increased from 0  $\mu\text{m}$  to 17.8  $\mu\text{m}$ . The thermal error in the lathe with CI bed with the cross-feed drive idling as per the loading cycle is 9  $\mu\text{m}$ . The experiments lasted for 360 min, as required by the standards, and the linearity for the  $x$ -axis thermal growth of both the lathe with CI bed and that with SREG bed at 40 °C has not been observed in a time span of 0 min to 360 min. Finally, the linear axis growth at 360 min of idle run in the lathe with CI bed is limited to 9  $\mu\text{m}$ , whereas in the lathe with SREG bed is 17.8  $\mu\text{m}$  a time span of 0 min to 360 min.

From the experiments, the lathe with the SREG bed exhibits 1.68 times higher thermal error at 20 °C and 1.88 times higher at 40 °C environment temperature than the thermal error in the lathe with CI bed. The higher thermal error in the lathe with the SREG bed is due to the more heat accumulation in the steel reinforcement. According to Weidlich and Nestmann [25], the thermal deformations in a machine tool with a polymer concrete bed is higher, and such deformations are reduced by improving heat conduction with the help of additional steel fixings. The measurements of temperature and deformations at required locations under different conditions and the analysis of the same are possible with a validated finite element modal. The development of the FEM is presented in Section 3.

### 3 DEVELOPMENT OF NUMERICAL MODEL FOR FEED DRIVE OF CNC LATHE WITH CI AND SREG BEDS

A numerical model is developed to investigate the thermal behaviour of the CNC lathes with a CI bed and SREG bed, under the influence of idle running of a cross-feed drive. The assumptions considered to perform the analysis are: 1) Internal heat generation is given as heat input for bearings and ball screw; 2) Heat flow is given as input for frictional heat generation in guideways; 3) Heat generated by air friction loss can be ignored because it is insignificant in comparison to other heat sources; 4) Small system structures such as nuts, holes, and so on are omitted; 5) Heat transfer through radiation is not considered; 6) On the bottom

of the machine tool, no thermal deformation in the  $x$ ,  $y$ , or  $z$  directions exist.

### 3.1 Modelling of Heat Sources with Analytical Heat Calculations

Since it is practically impossible to measure temperatures at locations of heat sources to serve as input data for numerical analysis, analytical models are used to estimate the generated heat and convection. The heat transfer mechanism from sources to other structures undergoes conduction, contact conduction, free convection, and forced convection. Fig. 8 represents the method of modelling heat for various heat sources with analytical equations. The heat sources are: 1) Heat produced due to the sliding of the carriage relative to the guide block; 2) Heat generated by the bearings; 3) Heat generated by the lock nut; 4) Feed drive motor electromagnetic heat losses. The model is considered to have an initial preload which is further considered as radial load ( $F_r$ ) and axial load ( $F_a$ ) on the angular contact bearing are 477.34 N, and 500 N respectively. The feed rate is 20 m/min.

The torque and frictional heat due to friction in the bearings is calculated by the given Eq. (1) [38]:

$$H_b = 1.047 \times 10^{-4} n M_b, \quad (1)$$

where,  $M_b$  is total frictional torque acting on the bearing, and  $n$  is the shaft rotational speed, total frictional torque,  $M_b = M_1 + M_2$ . Here  $M_1$  is load-related frictional torque and  $M_2$  is viscosity-related frictional torque.

$$M_1 = f_1 F_b d_m, \quad (2)$$

where

$$\begin{aligned} f_1 &= 0.001(P_0/C_0)^{0.33}, \\ F_b &= 1.4F_a - 0.1F_r, \\ P_0 &= 2.3F_r \tan \theta + F_a, \end{aligned} \quad (3)$$

$$M_2 = 10^{-7} f_0 V_0 n \left( \frac{2}{3} d_m^3 \right), \quad \text{when } v_0 n \geq 2000, \quad (4)$$

$$M_2 = 160 \times 10^{-7} f_0 d_m^3, \quad \text{when } v_0 n \leq 2000. \quad (5)$$

In Eqs. (2), (4) and (5), the diameter of the pitch circle ( $d_m$ ) of bearing is 33.75 mm,  $f_0 = 2$  and  $f_1 = 0.00043$  are the parameters related to the type, structure, force, and lubrication of bearings. Kinematic viscosity ( $v_0$ ) of lubricant is  $3510^{-6} \text{ m}^2/\text{s}$ , rotational speed ( $n$ ) is 3000 rpm. The calculated internal heat generation in the bearing using Eqs. (4) and (5) is 453,211.6 W/m<sup>3</sup>.

The frictional heat generation between the moving nut and the ball screw is another important heat source. Eq. (6) [39] is used to calculate the heat developed by ball screw. The efficiency of the screw nut ( $\eta$ ) is 95 %, the diameter of the screw nut ( $D_m$ ) is 20 mm Parameters 1 (angle  $\delta$ ) and 2 (angle  $\alpha$ ) in Eq. (7) are 28° and 8.53°, respectively. Rotational speed ( $n$ ) is 3000 rpm.

$$H_s = 0.01\pi n M_s, \quad (6)$$

where  $M_s$  is total frictional torque of the ball screw system,

$$M_s = \frac{(1-\eta)W \tan(\alpha + \delta) D_m}{2}. \quad (7)$$

From Eq. (6), the heat generation in screw nut ( $H_s$ ) has been evaluated as 170,283.48 W/m<sup>3</sup>.

Heat generation in guideways can be evaluated using Eq. (8) [39]. The coefficient of friction ( $\mu$ ) is 0.12, the normal force acting on the guideway ( $F_g$ ) is 500 N, and moving velocity ( $V$ ) is 20 m/min.

$$H_g = \mu F_g V. \quad (8)$$

From Eq. (8), heat generation in guideways ( $H_g$ ) has been evaluated as 20 W. Motor heat losses are

considered as 50 W, and the same is given as heat flow to the surface of the drive motor. For free convection around stationary surfaces, the convection coefficient ( $h$ ) is considered as 10 W/(m<sup>2</sup>·K) [19]. Average self-forced convection on rotary and reciprocating surfaces at the specified feed has been calculated as 35 W/(m<sup>2</sup>·K) and 27 W/(m<sup>2</sup>·K), respectively.

The heat transfer to the EG portion from reinforcement by considering joint contact resistance will be different in the condition without considering joint contact resistance, as depicted in Fig. 9. Hence, the joint contact resistance between steel reinforcement and epoxy granite structures has been evaluated and provided as joint contact conductance in the simulation. Contact conductance depends on the geometry, surface roughness, mean interface pressure, and joint temperature. Contact conductance is the inverse of thermal contact resistance developed in the joint. Eq. (12) is an analytical model developed by Bahrami et al. [26] for estimating the thermal contact resistance between metal and polymer and is considered in this work. Joint resistance is a summation of the thermal constriction/spreading resistance through the micro contacts ( $R_s$ ) and bulk resistance of the polymer ( $R_b$ ).

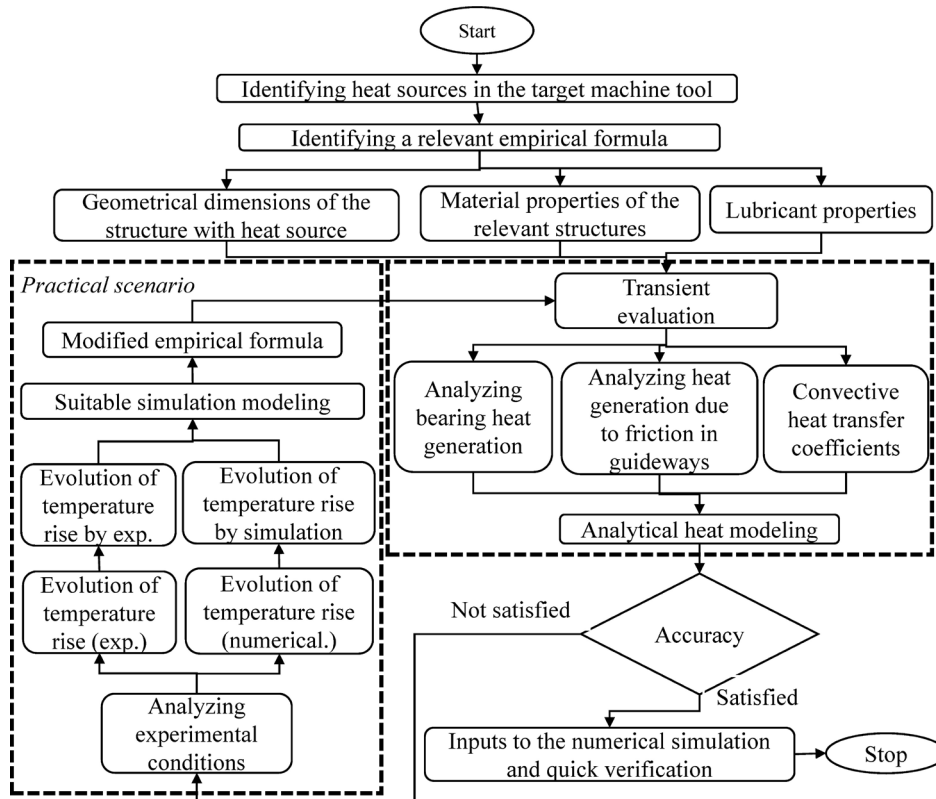


Fig. 8. Methodology for heat generation modelling

$$R_j = R_s + R_b, \tag{9}$$

$$R_s = \frac{0.565H_m(\sigma/m)}{k_s F}, \tag{10}$$

$$R_b = \frac{(t_0(1-(P/E_p)))}{(A_d k_p)}, \tag{11}$$

$$R_j = \frac{0.565H_m(\sigma/m)}{k_s F} + \frac{(t_0(1-(P/E_p)))}{(A_d k_p)}. \tag{12}$$

(m<sup>2</sup>·K)/W, and the joint contact conductance value, which is the inverse of joint contact resistance, is found to be 0.08 W/(m<sup>2</sup>·K).

Boundary conditions are applied to the lathe model in transient thermal analysis in ANSYS workbench. Later, for thermo-mechanical analysis, transient thermal analysis is coupled with static structural analysis. In experiments, throughout a 6 h time span, the temperature and x-axis thermal growth for the lathe have been collected. Similarly, for numerical transient analysis, total time span of 21,600 s (6 hours) was considered, and heat input values were provided at locations of heat sources as per the loading cycle.

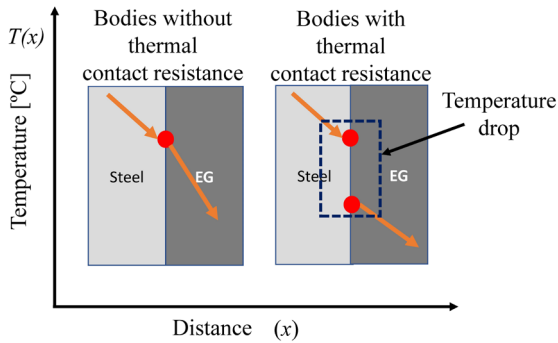


Fig. 9. Heat transfer without and with thermal contact conductance

Equivalent thermal conductivity of polymer and steel ( $k_s$ ) is considered as:

$$K_s = ((2k_m k_p) / (k_m + k_p)). \tag{13}$$

Polymer characteristics considered for epoxy are microhardness ( $H_m$ ) is 0.15 GPa, combined surface roughness ( $\sigma$ ) is 0.5  $\mu$ m, surface asperities slope ( $m$ ) is 0.14  $\mu$ m/m, thermal conductivity of steel ( $k_m$ ) is 50 W/(mK), minimum thickness of the polymer throughout the reinforcement ( $t_0$ ) is 5 mm. Contact pressure ( $P$ ) is 0.1 MPa, modulus of elasticity of the polymer ( $E_p$ ) is 20 GPa. Thermal conductivity of the polymer ( $K_p$ ) is 1.5 W/(mK). From the analytical Eq. (12), the joint contact resistance is estimated as 12.5

### 3.2 Numerical Thermal Investigations on CI and SREG CNC Lathe

A 3D Solid model of CNC lathe has been used for performing transient thermal finite element analysis (FEA) at 20 °C and 40 °C environmental temperatures for CNC lathe with CI and SREG beds.

Figs. 10a and b represent 3D meshed models of the lathe with SREG bed and lathe with CI bed, respectively. Other than the bed, which used the tetrahedron mesh method, the remaining structures used the hex dominant mesh method. A mesh convergence analysis was conducted to establish the optimal mesh size for the finite element model. The study concluded that a mesh size of 10mm was sufficient to produce accurate results and was therefore selected as the refined mesh size to ensure the reliability of the model. During analysis, calculated heat values were provided at the heat source locations in FE model. Convection (free air circulation) has been applied at the exposed boundaries. Figs. 10c and e depict the temperature distribution, Fig. 10d and f depicts the deformation under idle running of the cross-feed drive for lathe with CI and SREG beds at 20 °C, ETVC condition. The differences in temperature of various structures are responsible for deformation. The cumulative deformation of all

Table 3. Temperature comparison at sensor locations: experimental vs. numerical results

Sensor location	Lathe with CI bed at 20 °C			Lathe with SREG bed at 20 °C			Lathe with CI bed at 40 °C			Lathe with SREG bed at 40 °C		
	Exp.	FEA	% dev	Exp.	FEA	% dev	Exp.	FEA	% dev	Exp.	FEA	% dev
T 1 Ambient temperature	20	20	0	20	20	0	40	40	0	40	40	0
T 2 Top right LM block	24	25	4.2	26	27	3.8	43.5	46	1.2	46	48	4.3
T 3 Drive motor	29	29.2	0.6	32	33.3	4.1	48	51	6.2	49	52	6.1
T 4 Bed centre	23	22.5	2.2	22	21.5	2.3	43.5	43	1.2	42	41.5	1.2
T 5 Ball screw housing	24	25	4.2	25	26	4	44	45	2.3	44	45	2.3
T 6 Below turret	22	24	9.1	24	24.5	2.1	42	45	2.4	43.5	45.5	4.6

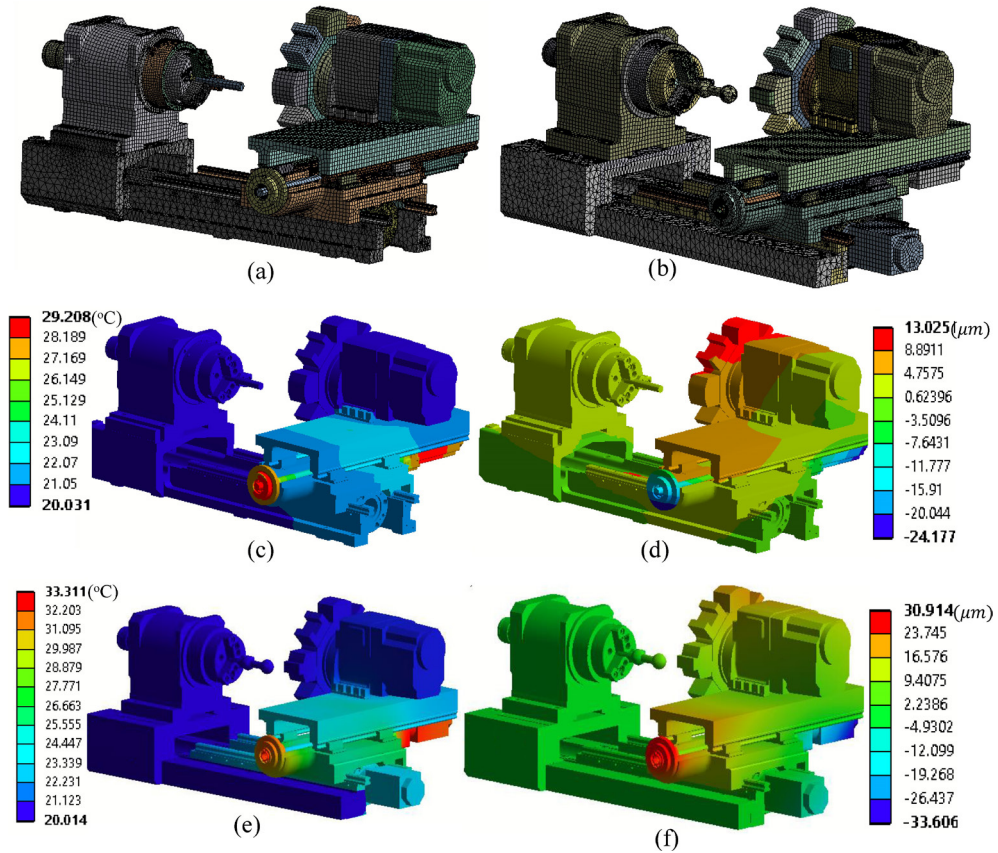


**Fig. 10.** a) 3D mesh model of lathe with CI bed, b) 3D mesh model of lathe with SREG bed, c) temperature distribution in lathe with CI bed, d) deformation of the lathe with CI, e) temperature distribution of lathe with SREG bed, and f) deformation of lathe with SREG bed (under cross feed-drive idle running at 20 °C)

**Table 4.** Deformation comparison at sensor locations: experimental vs. numerical results

Chamber temperature [°C]	Deformation measurement location	Deformation in lathe with CI bed [μm]			Deformation in lathe with SREG bed [μm]		
		Exp.	FEA	Deviation [%]	Exp.	FEA	Deviation [%]
20	TCP	8.8	9.5	7.9	14.8	16	8.1
40	TCP	9	9.4	4.5	17	17.2	3.4

structures is responsible for deformation at the TCP. Lead screws of both longitudinal and cross feed drives have significant temperature rises since they are nearer to the heat sources. The rise in temperature in all structures except the bed in the lathe with SREG bed is higher than the lathe with CI bed.

The effect of resistance causes a temperature rise in all locations, but in the case of the SREG bed, the temperature is less because of its lower thermal conductivity. Although there is not much temperature rise at TCP, the deformation at various structures causes a considerable deformation at TCP. The major structures contributing to TCP deformation are saddle, cross slide, bearing hub, bearings, cross feed drive guideways, and turret. The temperature obtained from

the different sensor locations in the experiment and temperature from same locations obtained from FEA are compared in Table 3. Deformation (x-axis growth at TCP) from experiments and FEA are compared in Table 4. Results from the FE analysis and experiments have been consolidated in Tables 3 and 4.

There is a good correlation between the results, and the numerical model developed is deemed validated. The validated simulation FEM model can be used for further analysis. The temperature and deformation in the lathe with CI bed and SREG bed from the simulation results are depicted in Fig. 10. Below the cross-feed drive bearing hub, saddle, structures in LF and the SREG bed are stationary.

Structures above the cross-feed drive (i.e., cross rail, turret, etc.) are subjected to motion.

These moving structures dissipate more heat due to self-forced convection. Therefore, the surface temperature of the top structure is less due to more heat dissipation. The temperature in the structures below the cross-feed drive is higher due to more heat conduction from nearby heat sources and less heat dissipation from these stationary structures. Even though the bottom structures experience higher temperature rise, they are constrained from expanding; the higher thermal growth of the top structures can be attributed to their free expansion at the top.

The transient state temperature and the thermal expansion from simulations at different locations are depicted in the Fig. 11. The total heat generated at the left and right bearings is the same but for the temperature of the right bearing is much higher than that of the left bearings because the right bearing is near the motor.

From Fig. 11, it is observed that the temperatures of the bed and steel reinforcement are not continuous and there are temperature drops due to thermal contact

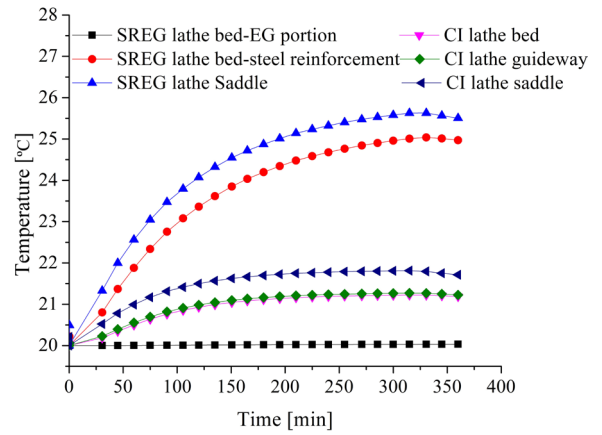


Fig. 11. Temperature profile of structures in lathe with CI bed and SREG bed at 20 °C

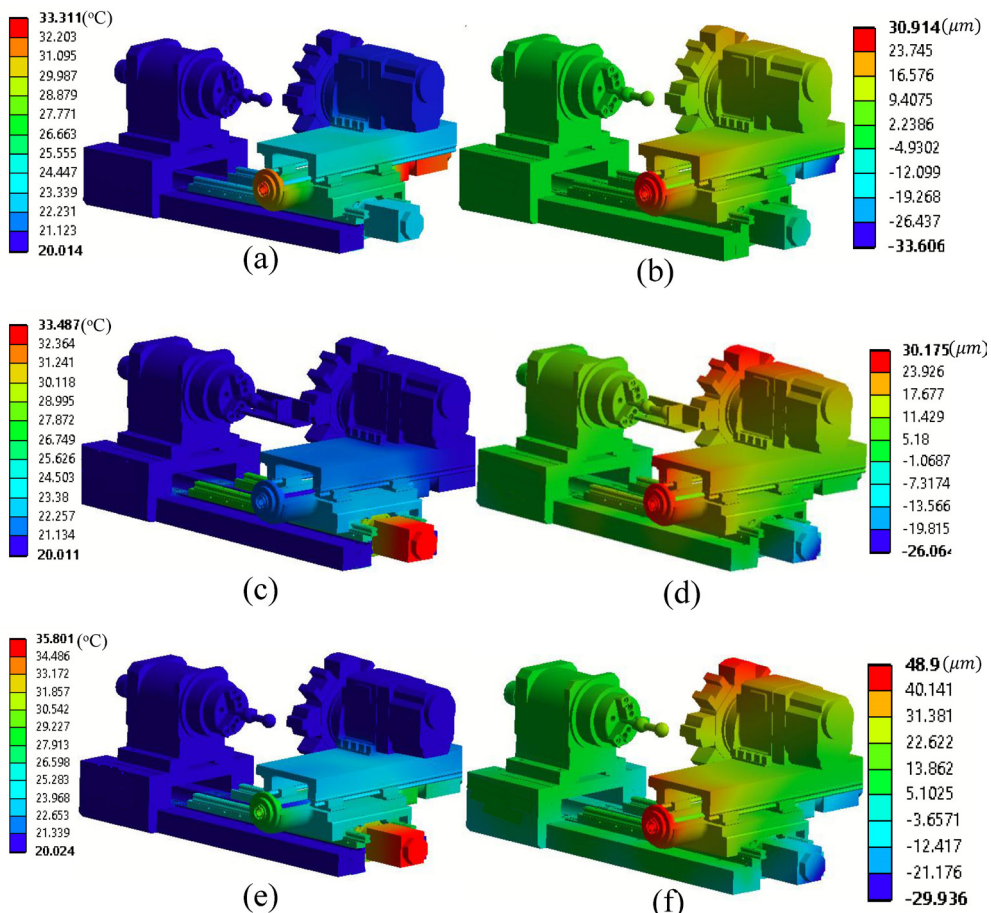
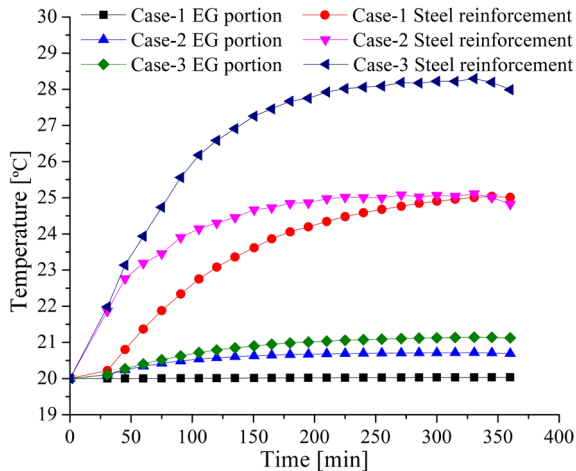


Fig. 12. Temperature distribution in lathe with SREG bed under 20 °C a) -Case-1, c) -Case-2, and e) Case-3; Deformation plot of lathe with SREG bed under 20 °C ETVc b) Case-1, d) Case-2, and f) Case-3

resistance. This can be attributed the high thermal contact resistance, which can also be referred to as low thermal contact conductance between steel reinforcement and EG. The motor deforms along the negative direction since it is exposed to convection and is free to expand in other directions, overhanging due to self-weight. Each of the two transits per period (one while moving downwards, one while moving upwards) leads to an increase in temperature, followed by a more gradual decrease due to heat diffusion.



**Fig. 13.** Transient temperature profile for EG and steel reinforcement in Case-1, Case-2 and Case-3

Motor temperatures in the lathe with SREG bed are 3 °C higher than the temperature at the same location in the lathe with CI bed. The steel reinforcement and EG structures are bonded together during fabrication, the heat flow from the top structures to the bed is not possible due to the difference in thermal characteristics of both materials. Consequently, a large temperature difference in bed and reinforcement has been observed. In the SREG bed, the EG portion and steel reinforcement are bonded together, and the reinforcement is provided to the bottom end of the bed. The temperature rise and expansion of EG in SREG bed are low, but it can be seen from the simulation result that the deformation of the EG is more than that of the CI bed which is due to expansion of corresponding bonded steel reinforcement.

#### 4 NUMERICAL SIMULATIONS UNDER IDLE RUNNING OF LONGITUDINAL FEED DRIVE AND BOTH FEED DRIVES

A combination of machining operations associated with feed and depth of cut will be responsible for a moment of both longitudinal and cross feed drives.

Therefore, the validated numerical model is used to analyse the thermal behaviour of the lathe with SREG bed under idle conditions of the longitudinal feed drive (Case-2) and both longitudinal and cross feed drives (Case-3). From temperatures and deformation of structures as shown in Fig. 12, it is clear that there is a more heat accumulation in steel reinforcement, which lead to higher thermal error in Case-2 and Case-3 as compared to Case-1. In Case-1, the heat generated in the cross-feed drive flows towards the structures above as well as below the drive, thus resulting in gradual increase in temperature of the steel reinforcement. In Case-2, since the heat sources are nearer to the SREG bed, due to more accumulation of heat in one side heat can flow from bottom to top. Therefore, a higher slope exists in the temperature profile of steel reinforcement at the beginning, as shown in Fig. 13. Similarly, in Case-3, one-sided heat flow from bottom to the top exists but with the same self-forced convection area as in Case-2.

From Fig. 13, it can be noted that the temperature of steel reinforcement in Case-3 is higher than that in Case-1 and Case-2. Idle running of LF will lead to more heat accumulation in the steel reinforcement than in Case-1, but after three hours, the temperature has been found to attain a steady state. No significant temperature rise was observed in EG in all the cases. Simultaneous idle running of both CF and LF has been found to result in a thermal error of 33  $\mu\text{m}$  which is 1.4 times higher than the thermal error in Case-2, and 1.9 times higher than that in Case-1. A similar trend has been observed in simulation results of feed drive with SREG bed at 40 °C. From temperatures and deformation of structures, it is clear that there is more heat accumulation in steel reinforcement, which leads to higher thermal error in Case-2 and Case-3 as compared to Case-1.

#### 5 CONCLUSIONS

Steel-reinforced epoxy granite structures have gained popularity due to their high damping characteristics and stiffness that is comparable or superior to that offered by CI structures. A systematic approach for thermal analysis of a CNC lathe with CI and SREG bed in closed ETVC conditions at 20 °C and 40 °C is presented in this article. The results reveal that the lathe with SREG bed exhibits a thermal error which is 1.68 times that of the lathe with CI bed at 20 °C and 1.8 times at 40 °C ETVC conditions. Furthermore, a thermo-mechanical FE model of the machine was developed. There was a high level of agreement when

the measured and simulated results were compared. Thermal analysis of the CNC lathe with the SREG bed reveals that it is more susceptible to thermal error than cast iron machines due to the accumulation of heat in steel reinforcement, which can be attributed to the low thermal conductivity of the surrounding epoxy granite portion. As a result, the thermal deformation of the steel structure in the bed is larger, and thus leads to higher thermal error. Simulation results reveal that idle running of LF develop 1.3 times than thermal error in idle running of CF. Idle running of both CF and LF develop 1.9 and 1.4 times than thermal error under idle running of CF and LF, respectively. This research initiative will make it feasible to apply strategies for thermal error reduction to machine tools with SREG structures.

## 6 ACKNOWLEDGMENTS

The authors acknowledge M/s Galaxy Machinery, India, Pvt Ltd, for the support and technical contributions. Authors' sincere thanks to AICTE-New Delhi, for providing fellowship through NDF program (National Doctoral Fellowship). The authors are sincerely thankful to PSG College of Technology-Coimbatore, for providing constant support in this research work. The authors wish to acknowledge the Advanced Machine Tool Testing Facility (AMTTF) for providing a thermal chamber to perform experiments.

## 7 FUNDING

The authors gratefully acknowledge the financial support for this research work by the Office of the Principal Scientific Adviser to the Government of India [Project sanction no. F.No.: Prn.SA/DRDP/MT/2010(G)].

## 8 REFERENCES

- [1] Ni, Y. Liu, X., Zhang, B., Zhang, Z., Li, J. (2018). Geometric error measurement and identification for rotational axes of a five-axis CNC machine tool. *Strojniški vestnik - Journal of Mechanical Engineering*, vol. 64, no. 5, p. 290-302, DOI:10.5545/sv-jme.2017.4581.
- [2] Selvakumar, M., Venugopal, P.R., Velayudhan, G. (2022). Optimization of a tuned mass damper location for enhanced chatter suppression in thin-wall milling. *Strojniški vestnik - Journal of Mechanical Engineering*, vol. 68, no. 5, p. 339-349, DOI:10.5545/sv-jme.2022.4.
- [3] Kepczak, N., Pawłowski, W., Kaczmarek, L. (2015). Cast iron and mineral cast applied for machine tool bed - dynamic behavior analysis. *Archives of Metallurgy and Materials*, vol. 60, no. 2, p. 1023-1029, DOI:10.1515/amm-2015-0254.
- [4] Saljé, E., Gerloff, H., Meyer, J. (1988). Comparison of machine tool elements made of polymer concrete and cast iron. *CIRP Annals*, vol. 37, no. 1, p. 381-384, DOI:10.1016/S0007-8506(07)61659-X.
- [5] Bedi, R., Chandra, R., Singh, S.P. (2013). Mechanical properties of polymer concrete. *Journal of Composites*, vol. 2013, art. ID 948745, DOI:10.1155/2013/948745.
- [6] Haddad, H., al Kobaisi, M. (2012). Optimization of the polymer concrete used for manufacturing bases for precision tool machines. *Composites Part B: Engineering*, vol. 43, no. 8, p. 3061-3068, DOI:10.1016/j.compositesb.2012.05.003.
- [7] Mula V.R., Thyla, P.R., Mahendrakumar, N., Praveena, K. (2021). Selection of resin and aggregates for particulate polymer concrete machine tool structures-A review. *Materials Today: Proceedings*, vol. 46, p. 8621-8628, DOI:10.1016/j.matpr.2021.03.595.
- [8] Mahendrakumar, N., Thyla, P.R., Mohanram, P.V., Kumaran, C.R., Jayachandresh, J. (2019). Study on static and dynamic characteristics of nettle-polyester composite micro lathe bed. *Proceedings of the Institution of Mechanical Engineers, Part L: Journal of Materials: Design and Applications*, vol. 233, no. 2, p. 141-155, DOI:10.1177/1464420716663568.
- [9] Möhring, H.-C., Brecher, C., Abele, E., Fleischer, J., Bleicher, F. (2015). Materials in machine tool structures. *CIRP Annals*, vol. 64, no. 2, p. 725-748, DOI:10.1016/j.cirp.2015.05.005.
- [10] Mahdi, F., Abbas, H., Khan, A.A. (2013). Flexural, shear and bond strength of polymer concrete utilizing recycled resin obtained from post consumer PET bottles. *Construction and Building Materials*, vol. 44, p. 798-811, DOI:10.1016/j.conbuildmat.2013.03.081.
- [11] Ferdous, W., Manalo, A., Wong, H.S., Abousnina, R., AlAjarmeh, O.S., Zhuge, Y., Schubel, P. (2020). Optimal design for epoxy polymer concrete based on mechanical properties and durability aspects. *Construction and Building Materials*, vol. 232, DOI:10.1016/j.conbuildmat.2019.117229.
- [12] Bajgirani, A.G., Moghadam, S., Arbab, A., Vatankhah, H. (2016). The mechanical characteristics of polymer concrete using polyester resin. *Journal of Fundamental and Applied Sciences*, vol. 8, no. 3, p. 571-578, DOI:10.4314/jfas.v8i3s.238.
- [13] D'Mello, J., D'Souza, A.G., Gowda, S.H., Pinto, D. (2019). Experimental investigation of compression, flexural strength and damping behaviour of granite particulate epoxy matrix composite. *AIP Conference Proceedings*, vol. 2080, DOI:10.1063/1.5092895.
- [14] Selvakumar, A., Mohanram, P. (2013). Evaluation of mechanical characteristics for mineral cast materials with varying resin content. *Journal of Engineering and Technology*, vol. 3, no. 1, p. 52, DOI:10.4103/0976-8580.107102.
- [15] Xu, P., Yu, Yh (2008). Research on steel-fibber polymer concrete machine tool structure. *Journal of Coal Science and Engineering (China)*, vol. 14, p. 689-692, DOI:10.1007/s12404-008-0444-z.
- [16] Suh, J.D., D. G. Lee, D.G. (2008). Design and manufacture of hybrid polymer concrete bed for high-speed CNC milling

- machine. *International Journal of Mechanics and Materials in Design*, vol. 4, p. 113-121, DOI:10.1007/s10999-007-9033-3.
- [17] Chinnuraj S., Thyla, P.R., Elango, S., Venugopal, P.R., Mohanram, P.V., Nataraj, M., Mohanraj, S., Manojkumar, K.N., Ayyasamy, S. (2020). Static and dynamic behavior of steel-reinforced epoxy granite CNC lathe bed using finite element analysis. *Proceedings of the Institution of Mechanical Engineers, Part L: Journal of Materials: Design and Applications*, vol. 234, no. 4, p. 595-609, DOI:10.1177/1464420720904606.
- [18] Mayr, J., Jedrzejewski, J., Uhlmann, E., Donmez, M.A., Knapp, W., Härtig, F., Wendt, K., Moriwaki, T., Shore, P., Schmitt, R., Brecher, C., Würz, T., Wegener, K. (2012). Thermal issues in machine tools. *CIRP Annals*, vol. 61, no. 2, p. 771-791, DOI:10.1016/j.cirp.2012.05.008.
- [19] Selvakumar, A., Mohanram, P.V. (2013). Evaluation of effective thermal conductivity for mineral cast structural materials using steady-state and transient methods. *Journal of Testing and Evaluation*, vol. 41, no. 4, p. 1-7, DOI:10.1520/JTE20120216.
- [20] Bryan, J. (1990). International status of thermal error research. *CIRP Annals*, vol. 39, no. 2, p. 645-656, DOI:10.1016/S0007-8506(07)63001-7.
- [21] Prabhu Raja, V., Thirumalaimuthukumar, M., Thyla, P.R., Shyam Kirthi, S. (2019). A strategy for minimization of thermal error in headstock assembly of CNC lathe. *Machining Science and Technology*, vol. 23, no. 1, p. 57-78, DOI:10.1080/10910344.2018.1466328.
- [22] Suh, J.D., Lee, D.G. (2004). Thermal characteristics of composite sandwich structures for machine tool moving body applications. *Composite Structure*, vol. 66, no. 1-4, p. 429-438, DOI:10.1016/j.compstruct.2004.04.065.
- [23] Tanabe, I., Takada, K. (1994). Thermal deformation of machine tool structures using resin concrete: Thermal behaviour of concrete bed of machine tool in fluctuating ambient temperature," *JSME International Journal. Ser. C, Dynamics, Control, Robotics, Design and Manufacturing*, vol. 37, no. 2, p. 384-389, DOI:10.1299/jsmec1993.37.384.
- [24] Neugebauer, R., Neugebauer, R., Drossel, W.-G., Ihlenfeldt, S., Al, E. (2012). Inherent thermal error compensation of machine tool structures with grated meneral casting, p. Art. 12053, 5, <https://publica.fraunhofer.de/handle/publica/377838>.
- [25] Weidlich, D., Nestmann, S. (2001). Kompaktführungen an Mineralgussgestellen. *Werkstatt und Betrieb*, no. 7-8, p. 120-123, <https://publica.fraunhofer.de/handle/publica/199233>
- [26] Bahrami, M., Yovanovich, M.M., Marotta, E.E. (2006). Thermal joint resistance of polymer-metal rough interfaces. *Journal of Electronic Packaging, Transactions of the ASME*, vol. 128, no. 1, p. 23-28, DOI:10.1115/1.2159005.
- [27] Dunaj, P., Powalka, B., Berczyński, S., Chodźko, M., Okulik, T. (2020). Increasing lathe machining stability by using a composite steel-polymer concrete frame. *CIRP Journal of Manufacturing Science and Technology*, vol. 31, p. 1-13, DOI:10.1016/j.cirpj.2020.09.009.
- [28] Dunaj, P., Dolata, M., Tomaszewski, J., Majda, P. (2022). Static stiffness design of vertical lathe with steel-polymer concrete frame. *International Journal of Advanced Manufacturing Technology*, vol. 121, no. 1-2, p. 1149-1160, DOI:10.1007/s00170-022-09391-x.
- [29] Venugopal, P.R., Dhanabal, P., Thyla, P.R., Mohanraj, S., Nataraj, M., Ramu, M., Sonawane, H. (2020). Design and analysis of epoxy granite vertical machining centre base for improved static and dynamic characteristics. *Proceedings of the Institution of Mechanical Engineers, Part L: Journal of Materials: Design and Applications*, vol. 234, no. 3, p. 481-495, DOI:10.1177/1464420719890892.
- [30] Venugopal, P.R., Kalayarasan, M., Thyla, P.R., Mohanraj, P.V., Nataraj, M., Mohanraj, S., Sonawane, H. (2019). Structural investigation of steel-reinforced epoxy granite machine tool column by finite element analysis. *Proceedings of the Institution of Mechanical Engineers, Part L: Journal of Materials: Design and Applications*, vol. 233, no. 11, p. 2267-2279, DOI:10.1177/1464420719840592.
- [31] Xu, P., Yu, Y.-H. (2008). Research on steel-fiber polymer concrete machine tool structure. *Journal of Coal Science and Engineering (China)*, vol. 14, p. 689-692, DOI:10.1007/s12404-008-0444-z.
- [32] Chen, T.-C., Chen, Y.-J., Hung, M.-H., Hung, J.-P. (2016). Design analysis of machine tool structure with artificial granite material. *Advances in Mechanical Engineering*, vol. 8, no. 7, p. 1-14, DOI:10.1177/1687814016656533.
- [33] Shi, H., Ma, C., Yang, J., Zhao, L., Mei, X., Gong, G. (2015). Investigation into effect of thermal expansion on thermally induced error of ball screw feed drive system of precision machine tools. *International Journal of Machine Tools and Manufacture*, vol. 97, p. 60-71, DOI:10.1016/j.ijmactools.2015.07.003.
- [34] ISO 230-3:2007. *Test Code for Machine Tools Part 3: Determination of Thermal Effects*. International Organisation for Standardization, Geneva.
- [35] Ruijun, L., Wenhua, Y., Zhang, H.H., Qifan, Y. (2012). The thermal error optimization models for CNC machine tools. *International Journal of Advanced Manufacturing Technology*, vol. 63, p. 1167-1176, DOI:10.1007/s00170-012-3978-6.
- [36] Xu, Z.Z., Liu, X.J., Kim, H.K., Shin, J.H., Lyu, S.K. (2011). Thermal error forecast and performance evaluation for an air-cooling ball screw system. *International Journal of Machine Tools and Manufacture*, vol. 51, no. 7-8, p. 605-611, DOI:10.1016/j.ijmactools.2011.04.001.
- [37] Li, Y., Zhao, W., Wu, W., Lu, B., Chen, Y. (2014). Thermal error modeling of the spindle based on multiple variables for the precision machine tool. *International Journal of Advanced Manufacturing Technology*, vol. 72, p. 1415-1427, DOI:10.1007/s00170-014-5744-4.
- [38] Babu, S.R., Raja, V.P., Thyla, P.R., Thirumalaimuthukumar, M. (2014). Prediction of transient thermo-mechanical behavior of the headstock assembly of a CNC lathe. *International Journal of Advanced Manufacturing Technology*, vol. 74, no. 1-4, p. 17-24, DOI:10.1007/s00170-014-5916-2.
- [39] Min, X., Jiang, S. (2011). A thermal model of a ball screw feed drive system for a machine tool. *Proceedings of the Institution of Mechanical Engineers, Part C: Journal of Mechanical Engineering Science*, vol. 225, no. 1, pp. 186-193, DOI:10.1177/09544062JMES2148.